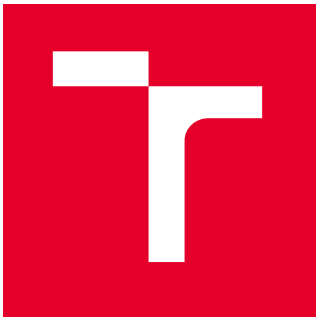

BRNO UNIVERSITY OF TECHNOLOGY

VYSOKÉ UČENÍ TECHNICKÉ V BRNĚ

FACULTY OF MECHANICAL ENGINEERING

FAKULTA STROJNÍHO INŽENÝRSTVÍ

INSTITUTE OF SOLID MECHANICS, MECHATRONICS AND BIOMECHANICS

ÚSTAV MECHANIKY TĚLES, MECHATRONIKY A BIOMECHANIKY

DEVELOPMENT OF RIG FOR TESTING FRICTION TORQUE OF LOW-SPEED BEARINGS IN VACUUM

VÝVOJ ZAŘÍZENÍ PRO TESTOVÁNÍ PASIVNÍHO ODPORU POMALUBĚŽNÝCH LOŽISEK VE VAKUU

BACHELOR'S THESIS

BAKALÁŘSKÁ PRÁCE

AUTHOR — **Ivo Lachman**

AUTOR PRÁCE

SUPERVISOR — **Ing. Martin Appel, Ph.D.**

VEDOUCÍ PRÁCE

BRNO 2024

BRNO UNIVERSITY OF TECHNOLOGY
FACULTY OF MECHANICAL ENGINEERING

Assignment Bachelor's Thesis

Institut:	Institute of Solid Mechanics, Mechatronics and Biomechanics
Student:	**Ivo Lachman**
Degree programm:	Mechatronics
Branch:	no specialisation
Supervisor:	**Ing. Martin Appel, Ph.D.**
Academic year:	2023/24

As provided for by the Act No. 111/98 Coll. on higher education institutions and the BUT Study and Examination Regulations, the director of the Institute hereby assigns the following topic of Bachelor's Thesis:

Development of rig for testing friction torque of low–speed bearings in vacuum

Brief Description:

Student's task is to develop a testing rig for testing low–speed bearings in vacuum. The rig shall monitor friction characteristics of the bearing with the use of highly precise torque measuring sensor. The device shall have the temperature sensors as well as the position sensor for accurate measuring of bearing current position. Student has to make a design proposal, select what components will be used and determine the measurement process. The proposal must always be reviewed and accepted by his mentor from Honeywell, who will give feedback to the student. The goal of this thesis is not to manufacture the device.

Bachelor's Thesis goals:

1) Conduct research in a field of measuring bearing friction torque.
2) Perform an analysis of possible causes that lead to a change of a bearing friction torque.
3) Propose a measurement methodology and method for evaluating results.
4) Design the testing rig and create an appropriate documentation, justify selection of critical components.

Recommended bibliography:

GREPL, Robert. Kinematika a dynamika mechatronických systémů. Brno: Akademické nakladatelství CERM, 2007. ISBN 978-80-214-3530-8.

Deadline for submission Bachelor's Thesis is given by the Schedule of the Academic year2023/24

In Brno,

L. S.

prof. Ing. Jindřich Petruška, CSc. Director of the Institute	doc. Ing. Jiří Hlinka, Ph.D. FME dean

Abstrakt

Tato práce se zabývá vývojem testovacího zařízení na testovaní nízkootáčkových ložisek vyrobených pro vesmírné aplikace. Testovaní musí být prováděno ve vakuu pro dosažení co nejpřesnějšího výsledku měření. Vedlejším cílem dále bylo znovupoužít co nejvíce již existujících komponent.

Summary

This thesis focuses on developing a testing rig for space grade low-speed bearings. Testing must be performed in a vacuum chamber to gain the most accurate measurements. Additional goal is to reuse as many already purchased components as possible.

Klíčová slova

Testovací zařízení, kuličkové ložisko, třecí moment

Keywords

Testing rig, ball bearing, friction torque

Bibliographic citation

LACHMAN, Ivo, *Development of rig for testing friction torque of low-speed bearings in vacuum*. Brno, 2024. Available from: `https://www.vut.cz/studenti/zav-prace/detail/157277`. Bachelor thesis. Brno University of Technology, Faculty of Mechanical, Institute of Solid Mechanics, Mechatronics and Biomechanics. Thesis supervisor: Martin Appel.

PROHLÁŠENÍ O PŮVODNOSTI ZÁVĚREČNÉ PRÁCE

Prohlašuji, že jsem závěrečnou práci s názvem *Development of rig for testing friction torque of low-speed bearings in vacuum* zpracoval samostatně a že jsem uvedl všechny použité informační zdroje.

DECLARATION OF AUTHORSHIP OF THE FINAL THESIS

I declare that this final thesis titled *Development of rig for testing friction torque of low-speed bearings in vacuum*, is my own work and the result of my own original research. I have clearly indicated the presence of quoted or paraphrased material and provided references for all sources.

Ivo Lachman

Brno . . . .

Děkuji všem svým kolegům ve společnosti Honeywell, za jejich znalé rady a především panu Ing. Vítkovi Nešporovi, který strávil nespočet hodin usměrňování mých nápadů, a svému vedoucímu práce panu Ing. Martin Appel, Ph.D. V neposlední řadě děkuji panu Ing. Martinu Brablcovi, Ph.D. za jaho šablonu v programu LaTeX, která mi velice usnadnila psaní práce.

Ivo Lachman

Contents

1 Introduction

Ball bearings are a key element in space mechanisms which are not only used in scientific research, but also in commercial applications. The commercial space business has seen a significant growth, where companies aim to build megaconstellation of satellites, that provide internet all around the world.

When designing a reliable mechanism for space application, proper methods must be used, such as simulations and analysis(e.g. Finite Element Method (FEM)). Despite all the progress made with simulation software and the complexity of analysis, that are made in the virtual environment, tests and validations are, and probably always will be, an important element in the design process of space mechanisms.

The space mechanisms are also unique in terms of the constraints that affect them. Typical constraints are the weight budget, i.e. the total weight of the mechanism with payload, or size budget, where the mechanism must fit into a pre-defined stay-in zone. But sometimes more critical are budgets such as power or thermal.

That is where analysis of the ball bearing performance comes in handy, because if properties such as power losses (torque losses) are measured and modeled correctly, optimizations can be done to make them lower. This could, for example, result in lower torque needed from a motor, that is directly affecting the power budget as well as the thermal budget or better accuracy that could be achieved with actuators with friction compensation.

If the bearing's friction model is known, a friction compensation can be added into the control software, ensuring greater precision, especially in low-angle scenarios, where the static and dynamic friction do not behave predictably. [1]

The goal of this thesis is to design a testing rig, that is able to measure and analyse the friction torque of the ball bearing, reusing as many already purchased in-house made components as possible. Also, the testing rig has to be able to accept different sizes of bearings, since a testing rig specialized for one type of bearing would not be cost-effective.

2 Friction torque in ball bearings

The friction torque generated by ball bearings is one of the most important aspects after the load capacity for maintaining desired precision of actuators. Excessive friction, i.e. friction torque, can lead to overheating of the bearing and it's surroundings, since heat dissipation is a serious problem in space mechanisms. That is because the lack of atmosphere that makes radiation the only way to loose the generated heat. This inverse in friction torque can shorten its lifespan as well as overload and damage the motor.

Analysis of the mechanisms are performed in virtual environments. Analysis using e.g. FEM are used to simulate the mechanism in various ways. Some of the performed analysis can be structural, modal and thermal. The digital twin of the mechanism however must be verified to be declared as accurate. To create a model corresponding to reality, performance of the bearing must be measured. The variables that create and lead to change in the friction of the ball bearing rolling elements are discussed in section 2.1. [1]

Bearings for space application are typically used under no loads during operation, except the axial preload, since operating in microgravity. The environment also affects the flow and evaporation (outgassing) of the lubricant, that can affect the lifespan of the bearing and the mission where it is used as well as the friction torque. Despite almost no loads during operation, when the mission is launched into space, the bearing must be able to withstand high vibrations and shock loads, which must not alter the predicted behaviour or lifespan in orbit. [2]

2.1 Friction generation

There are multiple factors when dealing with friction torque generation in ball bearings, but their influence on it may vary. This section is focused on what are the causes of friction generation as well as how to change them.

The torque loss can be also assumed as power, that the bearing converts to undesired energy in the form of heat. [2]

The partial losses, that in sum add up to the total torque loss, are defined by Herbert B. Singer in book Space Vehicle Mechanism: Elements of Successful Design as:

- *Retainer (cage) related losses.*
  - *Ball to pocket.*
  - *Retainer to land.*
- *Ball to inner and other ring related losses.*
  - *Shear in the Elastohydrodynamic lubrication (EHD) film due to slip between the load-carrying elements.*
  - *Pivoting in the EHD film in the contact area.*
  - *Hysteresis due to inelastic deformation of the metal parts in the contact zone.*
- *Lubricant related losses.*
  - *Churning due to plowing through "excess" of oil of grease.* [3]

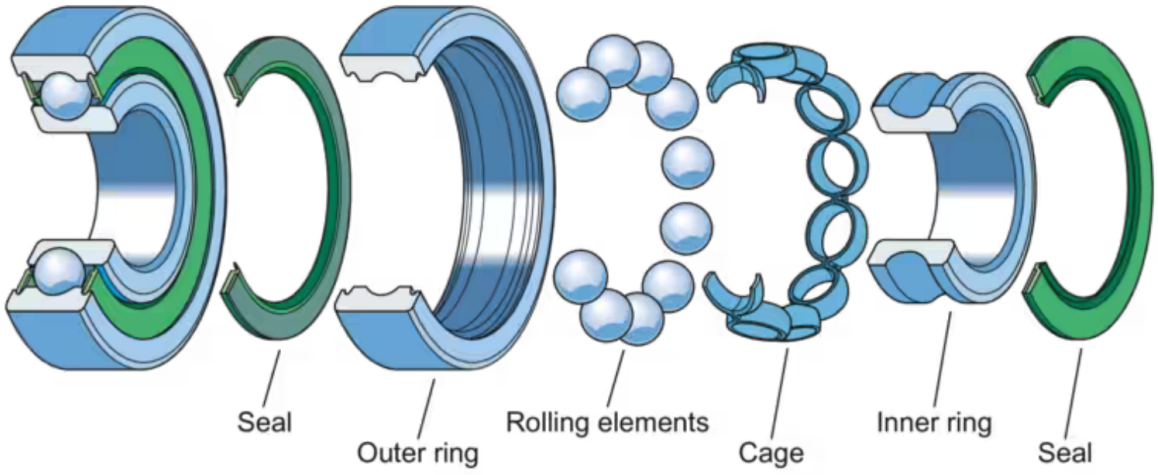

Figure 2.1: Ball bearing components. [4]

The ball bearings and their friction is also affected by their poor assembly. This fact is omitted, because only proper installation is considered. The typical composition of the ball bearing can be seen in figure 2.1.

Retainer related losses

The retainer related losses consists of losses created in the retainer pockets (on figure 2.1 called cage), where balls become unstable and increase the friction coupling between them and the retainer. This instability can be even heard (e.g. bearing *squeal* or *squeak*). This noise is caused by high frequencies, that are created due to the whirl frequency being typically ten times higher than the ball spinning frequency, because of the ball pocket clearance being usually ten times smaller, that the ball diameter. [2]

Retainer to land losses are typically small in comparison to other losses. They are created by the sliding of the retainer around the inner and outer ring. These losses can be higher due to high centrifugal forces acting on the retainer or when the ball to ball speed difference is high. Both of these effects occur at height speeds. [2]

Ball to inner and other ring related losses

Hysteresis losses are not dependent of the lubricant. They are created by heat loss that occurs when the ball deforms the outer and inner rings due to loads. Some of the energy, that goes into the deformation is then given back to the ball, since the hysteresis problem can be represented as a compressing spring, where some of the energy is stored and eventually released, and some is lost. The losses are directly related to the preload with function of $\frac{4}{3}$ power of the preload. [2]

Pivoting losses (also called traction) are similar to hysteresis losses in a way, that they are created by the ball "moving" material away (in case of hysteresis losses deformation is considered as "moving" material away). In this case however, only the viscous fluid e.i. lubricant is considered. The losses are created by high pressure in EHD contact zone. Research has shown, that these losses are indented of speed and are only dependent on the integral of the contact pressure over the contact area in the EHD film. For low speeds, this has been shown that a power a of preload is greater than one is the function of the losses. [2]

Lubricant related losses

Lubricant related losses are a function of viscosity, speed and excess lubricant and no good model has been found yet. The lubricant can be a grease or oil, where grease generally creates greater losses. The excessive oil can help to cool down the bearing, thanks to lowering the thermal resistivity, but also causes the bearing to heat more, so a good balance has to be found. To lower the torque losses at high speed, the best practise is to use low viscous oil and reduce the oil quantity to as minimum as possible. [2]

Preload conditions

In a space mechanism, bearings are typically axially preloaded to prevent unloading during launch. They are typically hard mounted, meaning that the preload is very stiff and the total preload force changes drastically with temperature, because of thermal expansion. That is why, on a space mechanism, heaters are typically installed around bearings with low Revolutions Per Minute (RPM) and a long period of no movement, to maintain

operation temperature and thus the nominal prelaod. The cold case (lowest operational temperature) is often the worst case for friction resulting from the preload related processes, because if the bearing compresses due to thermal expansion, the preload rises. [2]

Materials chosen for bearing's components as well as bearing's housing can change the behavior of thermal expansion. The best practise is, if it's possible, to match the materials, so that they expand together with no relative movement between them, because of the same coefficient of expansion. Though, to ensure this effect, the thermal gradient between each of the components has to be minimal. [2]

Thermal gradient is however typically a problem, because the bearing is, thanks to the ball's small contact surface area, a good insulator. This property can be changed with preload, where tests conducted agree with theory, that the thermal resistance of unlubricated ball bearings decreases exponentially with load and heat. Conductivity of used lubricants is another significant factor, that lowers the thermal resistance. [2]

Summary

The friction torque i.e. power loss created in a ball bearing is a influenced by many aspects and is a function of axial preload, axial and radial load, temperature and thermal difference between bearing parts, viscosity and "excess" of lubricant.

For lowering the bearings friction torque, preload has to be as minimal as possible and lubricant of low viscosity (typically oil) is advised to be chosen. Excess of the oil should be also chosen wisely, to minimize the friction torque. Heaters can be installed to heat the bearing during no operation in order to maintain the nominal preload state.

2.2 Torque measurement

There are many ways to measure the torque as with any other physical property, however for this thesis, not all the methods are presented, only those, that were seriously considered. Generally, torque can be measured directly or indirectly. For this thesis application, it does not matter if the method is direct or indirect, just as long as the desired precision is met.

The desired sensor chosen upon this research must measure *zero* torque, meaning it must be able to measure the torque from zero up to it's nominal value and it must be able to measure static torque as well as dynamic.

Strain gage method

Strain gage torquemeter utilizes four meral-foil gages placed on the surface of a torsion element bonded to a bridge. If a good mechanical bond is maintained between the surface of the sensor and the strain gage and if the surface (elastic structure) deforms linearly under applied torque, than the two of the most important aspects are met for the sensor to function properly. [5]

The Wheatstone Bridge (figure 2.2) is used to connect the strain gages that are used as variable resistors which resistance changes with the deformation caused by torque. The measurement is performed by applying voltage reference to the points A and C and measuring the differential voltage between points B and D as shown in figure 2.2. [6]

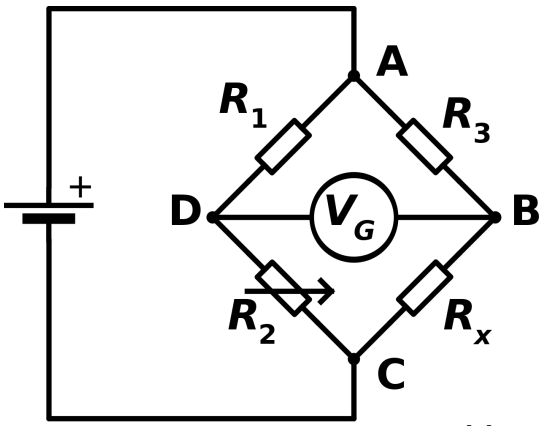

Figure 2.2: Wheatstone bridge. [7]

The torque sensor can then be placed on a shaft that is stationary or is rotating. If the shaft is stationary, than the cables from the sensor (strain gages) can be connected directly to an Analog to Digital Converter (ADC), otherwise the slip rings must be installed, to transfer the information form the rotating shaft. However, the slip rings can create a voltage drop, which needs to be compensated and could change with rotation, creating errors in measurement. This method can measure both static and dynamic torque. [5]

Twist angle deflection method

Twist angle deflection method fact, that materials under applied torque torsionally twist. The twist angle can then be measured and from the known torsion stiffness the applied

torque can be calculated. The angle can be measured with encoders or other sensors. The twist is not linear, however for small angles linearity is assumed with only negligible error. Generally, the angle is no greater than one or two degrees. To change the maximal torque, that the sensor can measure, the torsional stiffness or the distance between the two measured points of rotation can be made. This method can measure both static and dynamic torque. [5]

Electric motor torque measurement method

Indirect method of torque measurement is to measure the motor torque itself. Two methods are possible. Either measure the power of the motor and its revolutions, or use a motor torque constant KT (cΦ) and measure the electrical current. Both of these variants present certain obstacles, if precision torque measurement is required. [8]

If the method of motor power and revolutions is used, that the input power of the motor P_{mot} must be measured and the motor power losses P_{loss} (efficiency) of the chosen motor must be defined as precise as possible, to be able to convert the motor power to the real mechanical power on the motor shaft. To measure the shaft revolutions ω an encoder can be used and a high resolution must be chosen to meet the torque measurement precision criteria. The motor torque is then calculated using equitation 2.1. The disadvantage of this method is that at zero revolutions (stall of the motor), the torque cannot be measured. [8]

$$M_{\text{mot}} = \frac{P_{\text{mot}} - P_{\text{loss}}}{\omega} \tag{2.1}$$

If a DC motor is used and the motor torque constant cΦ is defined with required precision, then the only value needed to be measured is the electrical current I. The final motor torque M_{mot} is calculated using equation 2.2. [8]

$$M_{\text{mot}} = c\Phi \cdot I \tag{2.2}$$

Since both of these methods do not measure the torque on the measured element but on the element that creates the driving torque, every other torque loss that occurs during the transition from the motor shaft to the element must be measured and the offset needs to be added into the software. Also, the inertia would distort the measured values when changing the angular velocity, so additional software post-processing would have to be made and analysis of each rotary component inertia would have to be performed.

Summary

Chosen is the strain gage method for use in the testing rig. The sensor can be very compact and ADC with signal amplification is a component generally available. The benefit of measuring the torque generating element directly makes it a preferred option in comparison to other compact methods such as the motor torque measurement method for its reduced requirements of the torque loss analysis. More information about the specific torque sensor and ADC are given in subsection 3.2.2.

2.2.1 Testing methodology

An accurate friction bearing model is used to aid the position control loop. Research has shown, that the friction for small-angle characteristics typical for actuators can't be described simply by Coulomb model, a hysteresis loss or simplistic stick-slip function. The characteristics found more likely resembles that of a nonlinear spring, where the friction torque as a function of the angle. [1] [9]

Dahl's friction model is described as

$$\frac{dM_m}{d\theta} = \gamma \left[1 - \left(\frac{M_m}{M_s} \cdot sgn\left(\frac{d\theta}{dt}\right)\right)\right]^j, \tag{2.3}$$

where γ is a rest stiffness parameter of the system (Nm/rad), M_m is the measured friction torque (Nm), θ is the angle and j is the exponent to match the system. A value of $j \approx$ 1,5 is appropriate for ball bearings, but the value can be between 1 and 2. [1]

The steady-state friction M_s also called the Stribeck curve can be measured, as its definition implies, when the system is steady i.e. when the angular acceleration is zero. So, to measure it, the bearing shall be spun up from low revolutions up to the operating at nominal temperature. When the revolutions stabilize, the M_s can be measured. The stored value is the average of all of the measured values at current speed. [9] Than, interpolation with polynomial shall be done, which will result in function of describing the steady-state friction torque with dependency on revolution ω as $M_s(\omega)$.

This test shall be repeated for different operating temperatures with the same process, which will result in a function, that is also dependent on temperate T as $M_s(\omega, \mathrm{T})$.

To evaluated the rest of the unknowns (γ, j), the bearing shall be driven in a oscillatory manner. This method of measurement will trace out the hysteresis loop, that than can be interpolated and the values of γ and j are found. The modified equation 2.4 used in this experiment uses the function $M_s(\omega, \mathrm{T})$ determined during the previous test.

$$\frac{dM_m}{d\theta} = \gamma \left[1 - \left(\frac{M_m}{M_s(\omega, T)} \cdot sgn\left(\frac{d\theta}{dt}\right)\right)\right]^j, \tag{2.4}$$

where ω is the angular velocity, i.e. $\frac{d\theta}{dt}$. As with previous test, it shall be performed under multiple thermal conditions, so the variables would become a function of temperature T as $\gamma(\mathrm{T})$ and $j(\mathrm{t})$.

3 Testing rig overview

This chapter presents the hardware (electrical as well as mechanical) of the testing rig. Computer-Aided Design (CAD) visualisation of complete testing rig with Smallest possible bearing assembly 3.3.4 can be seen in figure 3.9.

The testing rig is based on a testing rig developed by Brno University of Technology (BUT) for Honeywell [10], with it's design having the driving motor beneath the tested bearing. Also, the same torque sensor is used (3.2.2), because it has been tested in a vacuum for this type of application. Not all similarities are based on BUT's testing rig. For example, the electrical motor driving the Measurement assembly 3.3.4 is placed outside and beneath the vacuum chamber and to transfer the torque into the vacuum chamber a rotary feedthrough is used. This solution is used because of technical trade-offs such as cooling of the motor and space constrains and does not have any connection with BUT testing rig.

The idea of the mounting Measurement assembly (3.3.4), i.e. the tested bearing, horizontally, is to make the axis of rotation parallel to the force of gravity. This way, minimal bending force is applied onto the shaft powering the measuring assembly and the shaft, that transmits the torque to the torque sensor. Also, this placement optimizes the bearing maximal size for reused vacuum chamber.

Requirements for the testing rig hardware are listed in subsection 3.1. Key parameters are listed in table 3.1.

Parameter	**Value**
Minimal tested bearing inner diameter [mm]	70
Maximal tested bearing outer diameter [mm]	190
Maximal tested bearing height [mm]	70
Moment of inertia of rotary parts [kg·m^2]	$\approx$ 0,022
Nominal revolutions [RPM]	400
Maximal measurable moment [Nmm]	1000
Precision pf torque measurement [Nmm]	$\pm$ 2,7
Torsion stiffness of elements in measuring chain [Nm/deg]	89
Theoretical speed-up time to nominal revolutions [s]	< 1

Table 3.1: Testing rig parameters and specifications.

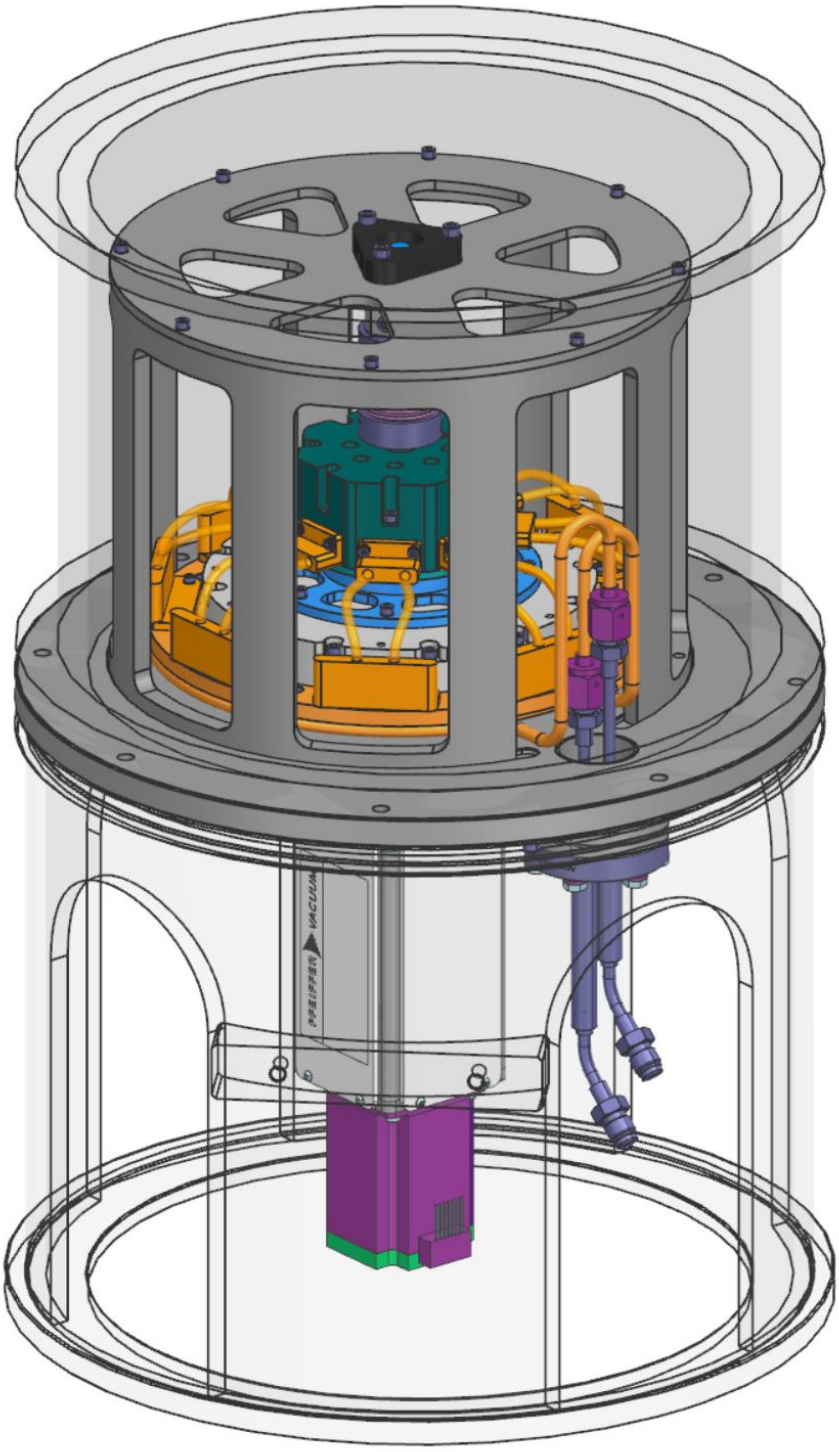

Figure 3.1: Testing rig top level assembly with installed measuring assembly for the smallest possible bearing.

3.1 Requirements

General requirements

3.1.0.1 Already purchased and in-house made components shall be used if no better alternative is presented.

3.1.0.2 Materials located in vacuum shall be only vacuum compatible i.e. low outgassing materials.

3.1.0.3 Temperature control of the test shall be possible.

3.1.0.4 Test's cold case (the lowest temperature possible) shall be -20 °C or lower.

3.1.0.5 Test's hot case (the highest temperature possible) shall be +60 °C or higher.

Mechanical requirements

3.1.0.6 Torque of 500 Nmm or greater shall be measurable.

3.1.0.7 Low-speed bearing shall be defined as a bearing operating at maximum of 300 RPM.

3.1.0.8 The test rig shall accept bearings with different sizes.

3.1.0.9 All holes shall be vented, to prevent air pockets (of barometric pressure).

3.1.0.10 The process of changing one bearing over another shall be easy and fast and shall not require special tools.

Electrical requirements

3.1.0.11 The minimal resolution of the torque sensor shall be 5 Nmm.

3.1.0.12 The minimal resolution of the encoder shall be 10 bit or $\approx$ 6,1 mrad.

3.1.0.13 The minimal resolution of the temperature sensor shall be 0,5 °C.

3.1.0.14 Temperature must be measurable over the entire defined range.

3.1.0.15 If Printed Circuit Board (PCB) is designed, all components shall be hand solderable.

3.2 Electrical hardware

Since plug-and-play products typically cost more than in-house developed solutions, the goal of the electrical hardware is to minimize labor, as well as component costs. Result is to use the breakout board modules, that need to be wired and programmed and do not work as is. The selected path applies hardware, that requires minimum effort to setup and can be assembled from off-the-shelf components.

Electrical requirements are listed in section 3.1.

Hence, with this in mind, PCB is designed (figure 3.2) to serve primarily as a breakout board for the chosen microcontroller. The PCB with all of its components was named Data Acquisition Board (DAB).

DAB's supply voltage is 12 V DC and it is based on 3V3 TTL logic. Microcontroller Teensy 4.1 [11] is used. Its 600 MHz processor with 32bit architecture is overpowered for this application. Teensy was chosen for it's compatibility with Arduino libraries that might not be as optimized as custom code, since the Teensy is overpowered, it's not a problem and the usage of these libraries will make programming easier and faster. Teensy also has build-in SD card, that can be used to store data locally, but also connection to programs such as LabVIEW is supported and can be established trough serial communication (USB).

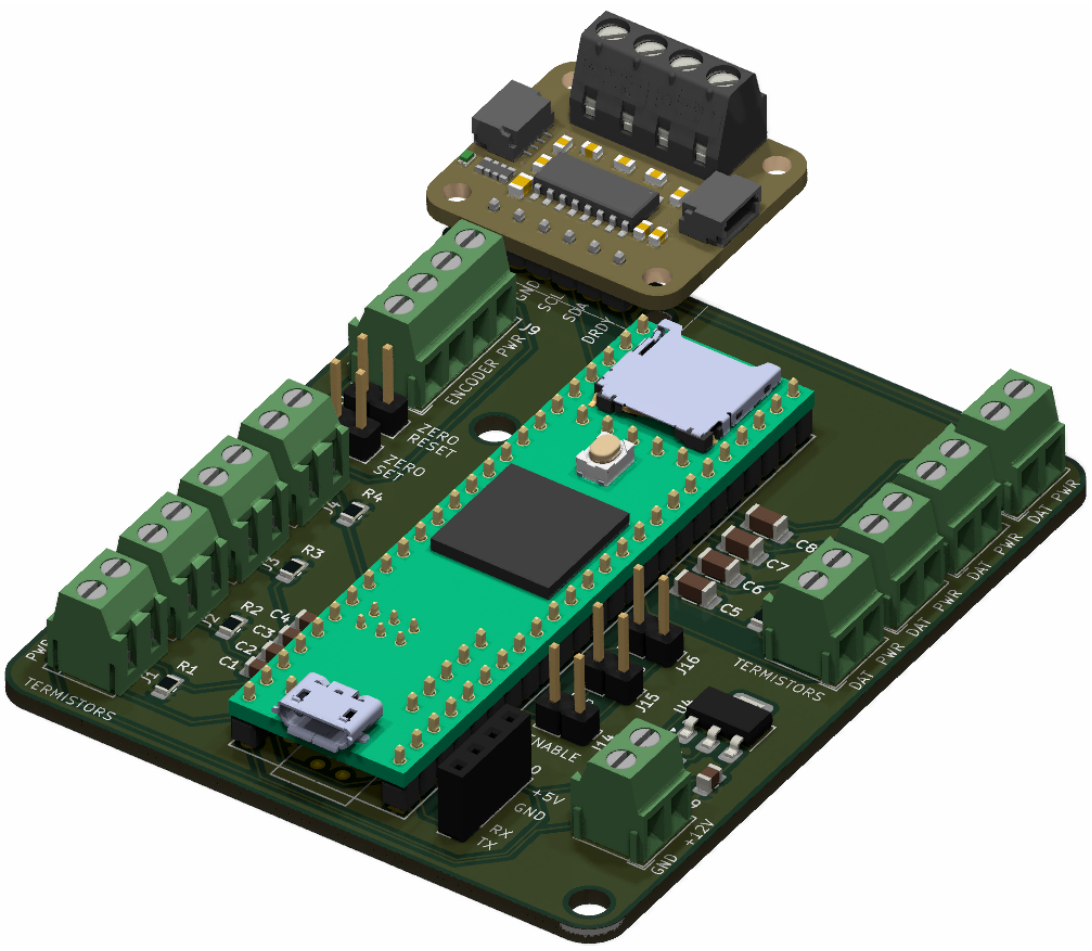

Figure 3.2: PCB KiCad 3D view rendered image.

3.2.1 PCB

The PCB is a component outside of the vacuum chamber, thus requirement 3.1.0.2 is not applicable. The board is designed with open source program KiCad EDA [12]. The board has not been manufactured yet in the time of writing this theses and all the pictures were created using the KiCad's 3D rendering feature (figure 3.2).

This one layered board with dimensions of 74.5 x 62 mm can be secured with two M3 screws. All components can be hand soldered as per requirement 3.1.0.15.

Some components use the 12 V supply voltage directly, and for others there is a linear voltage regulator, that lowers the voltage to 5 V. From there the voltage is lowered again by built-in voltage regulators of each component to 3,3 V. This method of daisy-chaining of linear voltage regulators may not be as efficient as using step-down voltage regulators, but it is very simple and since the board does not need much power, this approach is sufficient for this low power application. The board parts and pinout are described in figure 3.3. Each connector has described its functionality in silkscreen layer of the board.

In figure 3.3, pins for the stepper motor driver can be seen. The first idea was to control the motor from the DAB itself. This solution turned out to be more complicated that expected, so an external driver is used (see subsection 3.2.3). As the copper tracks were already routed at this stage, the connections were left on the board.

For additional information about PCB see attached files.

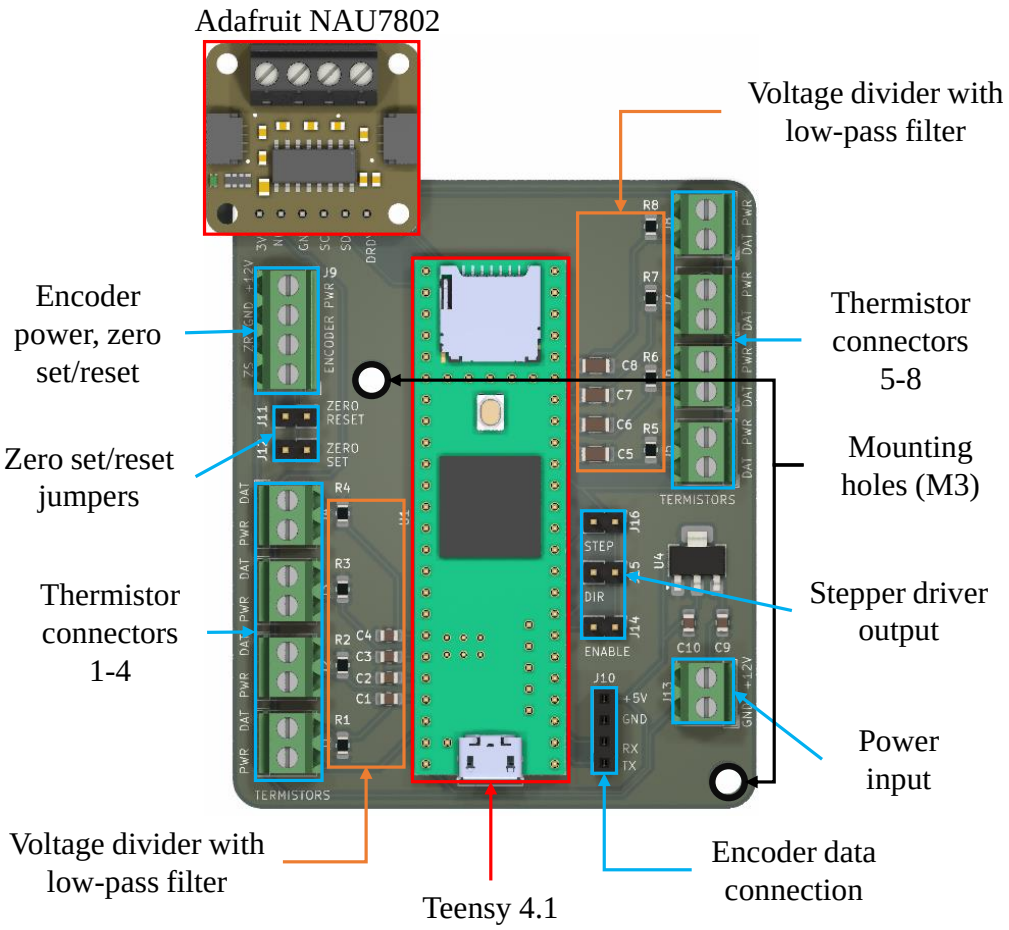

Figure 3.3: Board components overview.

3.2.2 Sensors

Torque sensor

Sensor TQM201 [13] made by Omega (figure 3.4) has been used for its verified performance in a vacuum by BUT [10]. The body is made of stainless steel and using the Wheatstone bridge [6], it can be read by Adafruit's ADC with amplification frontend board using Nuvoton's NAU7802 [14] specifically made for such application. All key information can be found in 3.2.

Figure 3.4: TQM201 torque sensor. [13]

Adafruit's board (figure 3.5) was selected for its price, I2C communication and high quality C++ and Arduino.h compatible libraries, provided by Adafruit as well. Other benefits are its internal voltage reference for ADC and stable voltage supply for the torque sensor. It has a high definition 24 bit ADC converter with maximum reading speed of 320 Hz and build-in software filtering. Only 12 Effective Number of Bits (ENOB) are needed, to meet the requirement 3.1.0.11.

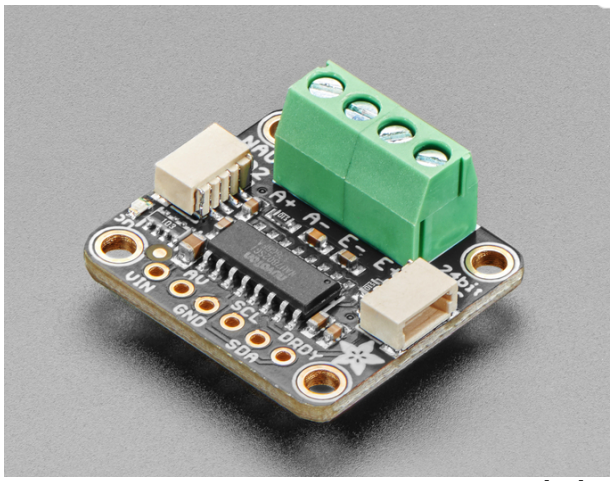

Figure 3.5: Adafruit's NAU7802 board. [14]

Technical information is listed in table 3.2.

TQM201	
Nominal torque [Nmm]	1000
Safe torque overload [Nmm]	1500
Voltage output [mV/V]	0,2
Accuracy [%]	±0,2 Full-Scale Output (FSO)
Linearity [%]	±0,15 FSO
Hysteresis [%]	±0,10 FSO
Operating Range [°C]	-54 to 107
Compensated Temp Range [°C]	16 to 71
NAU7802	
ADC resolution [Bit]	24
Maximal sampling rate [Hz]	320
Torque per ADC step (bit) [Nmm]	$166.89 \cdot 10^{-6}$
Maximal signal amplification (gain) [-]	128
Gain error [%]	± 0.01 Full Scale (FS)
Integral nonlinearity [%]	± 0,0015 FS
ENOB (@4.5V and gain 128)	19,97
Combined parameters	
Total error FSO [%]	± 0,27
Total error [Nmm]	± 2,7
Used bits [-]	18
Torque per ADC step (bit) with used bits [Nmm]	$2.81 \cdot 10^{-3}$

Table 3.2: Torque and ADC sensor information.

Encoder

Encoder is used to determine the position as well as the bearing's spin speed, though this component is not necessary. It will not be used to drive the actuator in a closed control loop. Stepper motor (used to drive the assembly) is very precise so it can be used in open loop without a problem. The slip between the motor and measured bearing is created in the magnetically coupled rotary feedthrough (3.3.1) and encoder is able to detect it, so the measured angle is the real bearing angle.

Celera Motion's IncOder Core is an absolute inductive encoder that was chosen for its zero torque loss, measuring precision, required low mounting precision, vacuum certification and no special calibration requirement. The absolute zero position can be set and reset manually using jumpers on the board, but for this thesis's application this feature is not used.

The encoder is used in configuration CORE-3-70-101001-SSI1-PR2 [15] (figure 3.6), using SSI communication with RS422 compatible hardware. To be able to read the encoder data, RS422 to TTL converter is used [16] and is connected to UART port via logic level converter [17] that lowers the voltage. Resolution of 10 bits is compliant with 3.1.0.12. Lower resolution was not available. The connection to the DAB is through electrical feedthrough.

Figure 3.6: Induction encoder IncOder CORE. [15]

Important features and values are listed in table 3.3.

Resolution [Bit]	10
Accuracy [arc sec]	125
Absolute [-]	Yes
Maximal revolutions [RPM]	10000
Internal update period [µs]	100
Maximum radial misalignment [mm]	± 0,2
Maximum axial misalignment [mm]	± 0,35

Table 3.3: Encoder information.

Temperature sensor

The PCB has a total of eight ports for Negative Temperature Coefficient (NTC) thermistors, which are used to measure the temperature inside the vacuum chamber. To read the temperature, microcontroller's internal 10bit ADC and voltage dividers are used. Every NTC can measure through the entire range per requirement 3.1.0.14. An in-built low-pass RC filter with time constant of $\approx$ 470 ms is used. This slower time constant improves signal noise immunity. Thanks to thermal processes having longer time constant than elector-mechanical processes (in range of seconds or even minutes), chosen time constant will not make the signal (temperature change) delayed.

Thermistor RTS103C1R2M3L102 [18] (figure 3.7) is used, as it can be easily mounted using only one screw. Relevant information may be seen in table 3.4.

β [K]	3977
Resistance @25 °C [kΩ]	10
Tolerance of thermistor [%]	2
Tolerance of resistor in series [%]	1
Temperature resolution with nonlinearity in mind [°C per ADC step]	0,27
Temperature uncertainty [°C]	± 0,006
Mounting screw [-]	M3
Time constant of RC filter [ms]	470

Table 3.4: Thermistor relevant information.

The chosen thermistor is not linear (see figure 3.8) in all of it's range. Software calculates the temperature using floating point to overcome this nonlinearity.

Figure 3.7: NTC thermistor RTS103C1R2M3L102. [18]

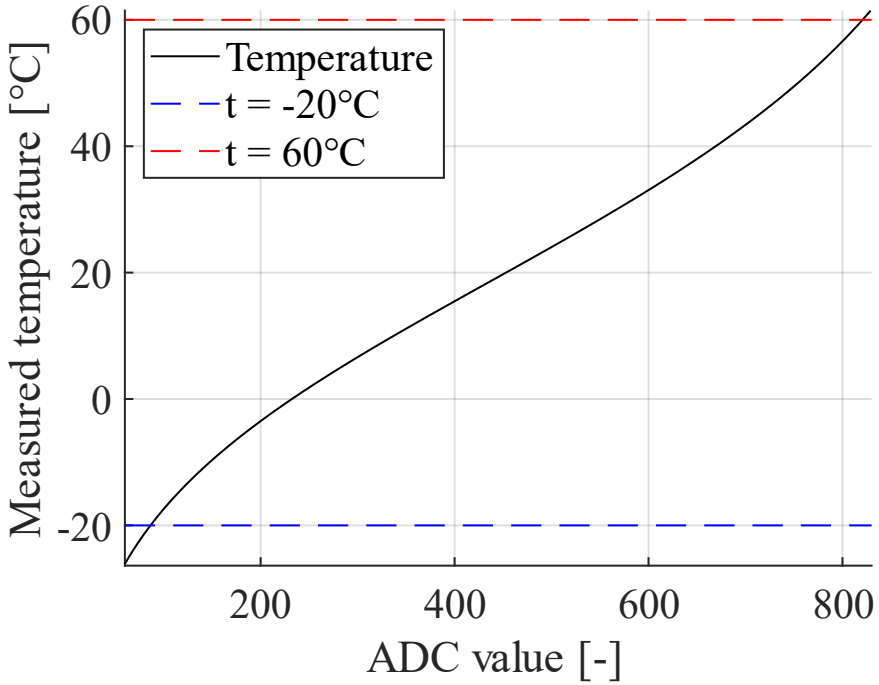

Figure 3.8: Entire meassuring range of used NTC thermistor.

It is advised to calibrate the thermistors for better precision, since both thermistor and resistor have some uncertainty, so readings from all of the channels will be distorted without the advised calibration.

3.2.3 Actuator

A stepper motor [19] is used, being permanently connected to rotation a feedthrough, that transfers its torque into a vacuum chamber (additional information in subsection 3.3.1, in which the reasoning for such a solution is given). Technical information is given in table 3.6.

In the first solution, that was proposed, the stepper motor was supposed to be controlled by DAB. That turned out to be a more complicated solution than expected, so a stepper controller 8SMC5-USB [20] is used instead. This controller also meets the requirement 3.1.0.1. The manufacturer provides software for the driver, which will control the motor in an open loop configuration. Micro-stepping is used to dampen the torque ripple effect. An IO synchronization can be used for DAB, but for that current proposed setup it is not.

The stepper motor is powered with 48 V and can consume up to 4,2 A. The stepper controller can only deliver 3 A of current, so a reduction of torque is expected.

3.3 Mechanical hardware

The testing rig can be divided either by operating pressure - vacuum/atmospheric, or by its relative speed - rotary/stationary. In figure 3.9, all of the components inside the red box are in the vacuum. In figure 3.10, all the green parts are rotating, hence are considered to be the rotary. More attention to the rotary parts is payed in subsection 3.3.1.

Mechanical requirements are listed in section 3.1.

General dimensions of the vacuum chamber were fixed, because the first decision was to reuse the vacuum chamber lid. It is important to note, that the lid of the chamber is equipped with various feedthroughs as well as port for the turbo-molecular pump, that are not displayed in the CAD (e.g. figure 3.9). Electrical feedthroughs on the vacuum chamber lid will be used to connect electronic components to DAB.

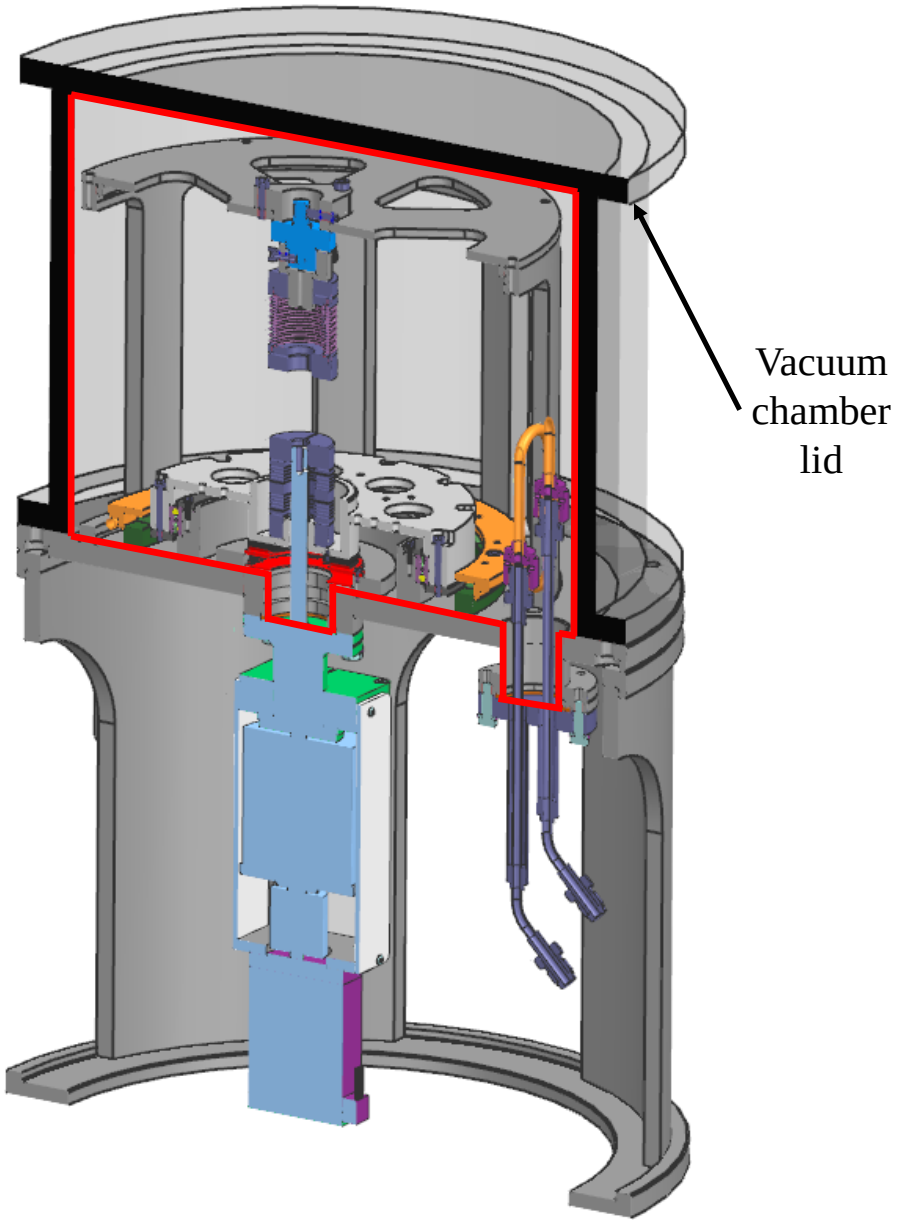

Figure 3.9: Testing rig - vacuum and atmospheric part of the rig (vacuum in red box). Shown without the Measuring assembly (3.3.4.

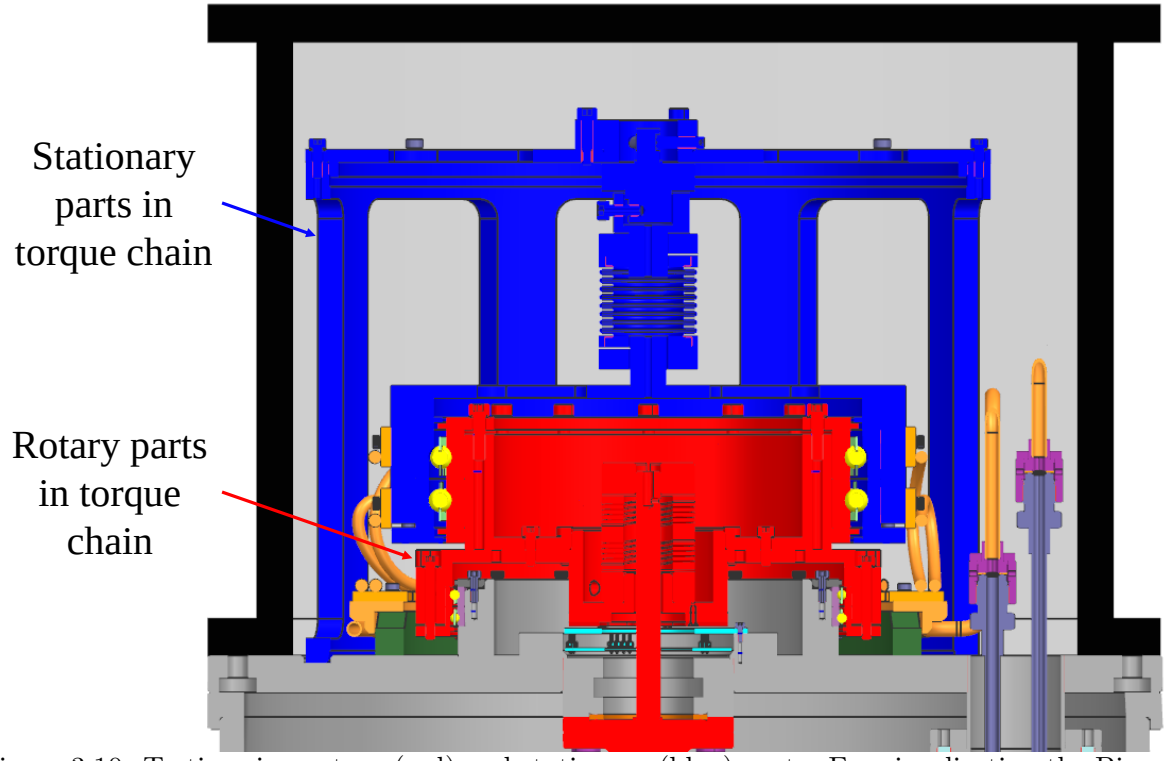

Figure 3.10: Testing rig - rotary (red) and stationary (blue) parts. For visualisation the Biggest possible bearing assembly (3.3.4) is shown

Honeywell parts

Parts that are not made for this thesis will not have resources such as datasheets and drawings referenced. The goal is to retrofit existing parts per requirement 3.1.0.1 and these components are only shown in figures to illustrate how the final assembly will look like.

Materials

Only three types of materials are used, if only machined parts are considered. Stainless steel AISI 304 (EN 1.4301) is used exclusively. For the thermal plate (subsection 3.3.3) copper alloy AMPCOLOY 940 is used. For all non-metallic parts that were machined, Epoxy Glass G10 FR4. Internal material sources were used to chose the materials, so the original sources can't be linked. All chosen materials for machining are in compliance with requirement 3.1.0.2.

3.3.1 Driving assembly

The driving assembly (figure 3.11) serves as a baseplate to which all other components are mounted and also is the hatch of the vacuum chamber lid. The baseplate itself has two feedthroughs, one to transmit rotation and other for fluids, that are connected through standardized welded flanges. The rotary feedthrough was positioned 15 mm eccentric to the axis of the baseplate, as seen in figure 3.12, to maximize the largest possible bearing's diameter.

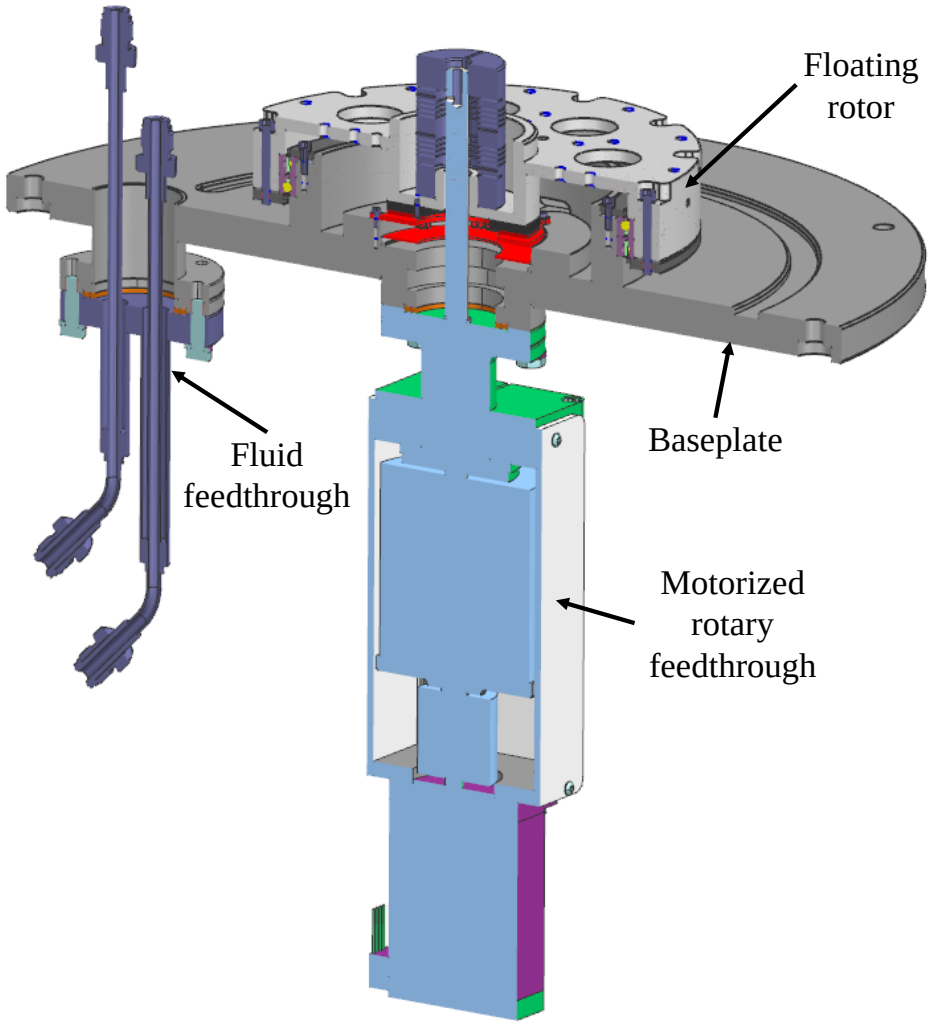

Figure 3.11: Driving assembly.

The floating rotor is connected through a bearing to the baseplate to which the measurement assembly 3.3.4 can be mounted. On the other side it is connected through flexible shaft coupling made from stainless steel to shaft of rotary feedthrough. Encoder rotor (3.2.2) is mounted to the bottom side with a non-metallic separator. The nonmetallic separator is also used for distance compensation, since the encoder rotor needs to have a certain distance from the encoder stator (table 3.3).

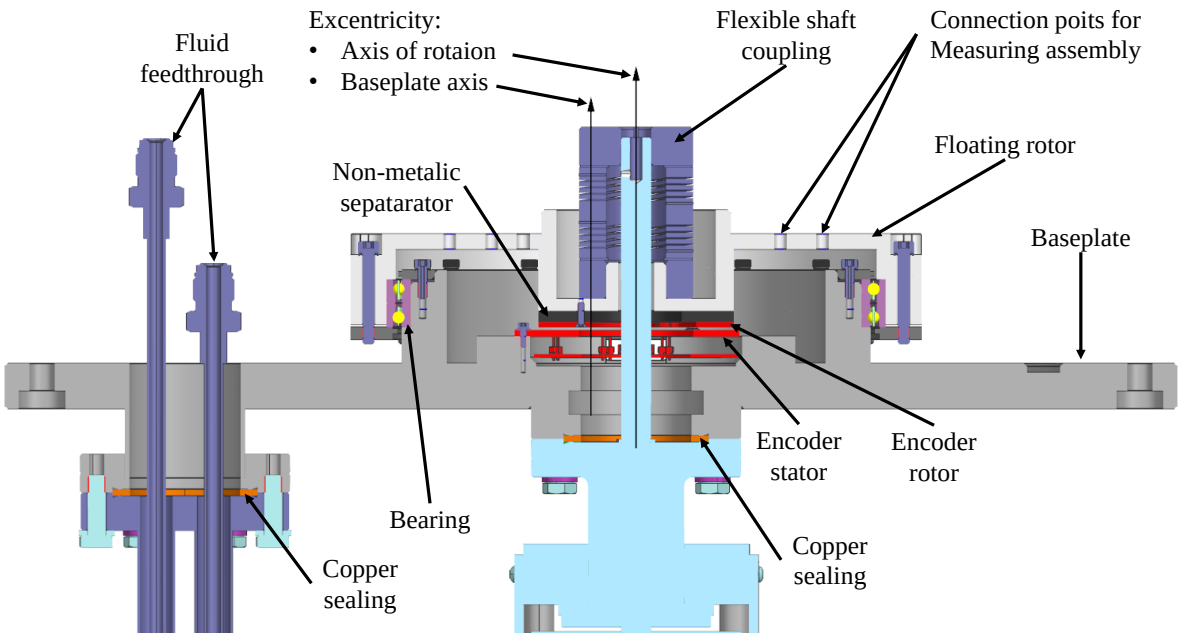

Figure 3.12: Driving assembly, detailed cross section.

Supporting bearing

SKF thin section bearing was chosen, for its small dimensions and load handling capacity. The exact bearing model number is SKF KDN.S15008BY0A [21] (cited bearing has the same dimensions, but it is in different configuration). It is used in back-to-back configuration for better rigidity. Both of the bearings are matched, so the preload set from manufacture, is created by pressing the inner rings. It is secured with screws, that are distributed to create even preload pressure, and it connects the baseplate to the floating rotor. Chosen preload prevents bearing's unloading. Overview of bearing's properties can be found in table 3.5. All calculations were done using internal tool (the analysis can be found in the attached files).

Inner (bore) diameter [mm]	150
Outer diameter [mm]	166
Width [mm]	8.001
Contact angle [deg]	30
Rolling bearing type	Angular contact paired-duplex back-to-back (type B)
Material (bearing / cage)	Bearing steel / brass
Estimated lifetime [h]	57 571
Static safety factor [-]	63,2
Estimated starting torque [Nm] (± 50%)	0,25

Table 3.5: Bearing parameters.

Rotary feedthrough

First design of the testing had the motor powering in the driving assembly placed in a vacuum. This solution was abandoned early, because there is not enough space in the vacuum chamber to fit the motor inside. Also, if the motor is in the vacuum it has to be specifically made to function in a vacuum environment e.g. use low outgassing materials (3.1.0.2). Additionally, cooling of the motor could be a problem, so moving this component to atmospheric part of the testing rig is, from a thermal point of view, a preferred solution.

To transfer the torque into the inside of the vacuum chamber a rotary feedthrough is used. At the beginning of the search for a rotary feedthrough, two variants emerged - with and without a motor. In the end, rotary feedthrough with a motor is used to simplify the manufacturing and assembly process.

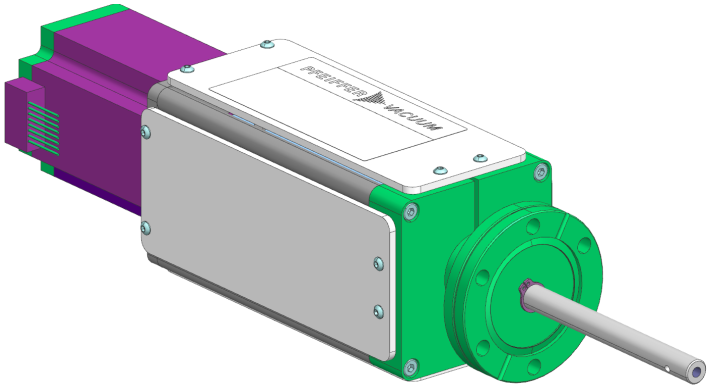

Figure 3.13: Rotary feedthrough. Visualized in CAD.

The used feedthrough is magnetically coupled rotary feedthrough 420MRM040-m [19] from Pfeiffer Vacuum. Technical specifications are listed in table 3.6. All parameters are in compliance with mechanical requirements in section 3.1.

The torque ripple will be dampened by the magnetic coupling, but to minimize it, a driver with micro-stepping is used (section 3.2.3).

Parameter	**Value**
Speed [rpm]	≤ 500
Torque [Nm]	3
Current [A]	4.2
Input voltage [V]	28 - 48
Angle resolution [deg]	0,45
Steps per revolution [-]	800
Connection flange	DN 40 CF
Motor type	2-ph stepping motor
Transmission	Note used
Coupling	Magnetic

Table 3.6: Rotary feedthrough, mechanical parameters.

3.3.2 Torque sensor assembly

This assembly contains the torque sensor and can be seen in figure 3.14. The torque sensor transfers the torque generated by the measured bearing to the flange through compensator connected to the stand, which holds it in place. On the other side the sensor is connected to flexible bellows coupling through an adapter.

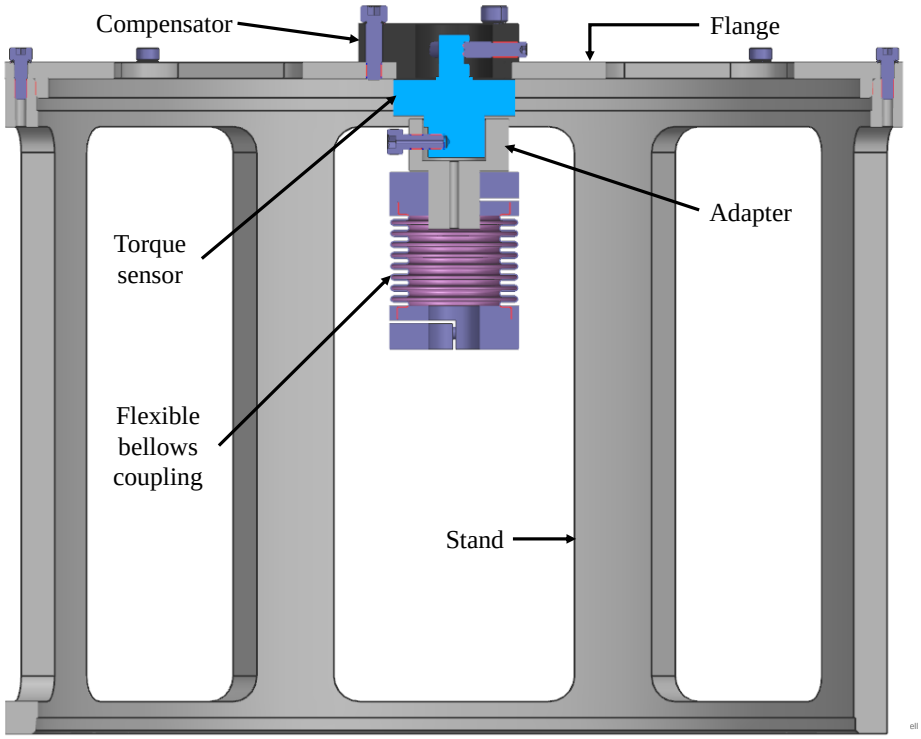

Figure 3.14: Torque sensor assembly.

Nonconcentricity of driving assembly (3.3.1), measurement assembly (3.3.4) and torque sensor is compensated by three flat surfaces on the torque sensor. They are connected to the compensator through three set-screws. The misalignment is compensated during installation of the measuring assembly, using 3D printed plastic parts witch holds the flexible bellows coupling locked, thus making it marginally more stiff. After that the three screws are tightened in a pattern ensuring no axial stress on the torque sensor. For best results two dial indicators shall be used, spaced 90 degrees apart as seen in figure 3.15. After the installation, the 3D printed plastic piece must be removed.

This installation of the torque sensor is required, because nonconcentricity of the measurement assembly (3.3.4) together with the torque assembly, may be greater than what the flexible bellows coupling can compensate for.

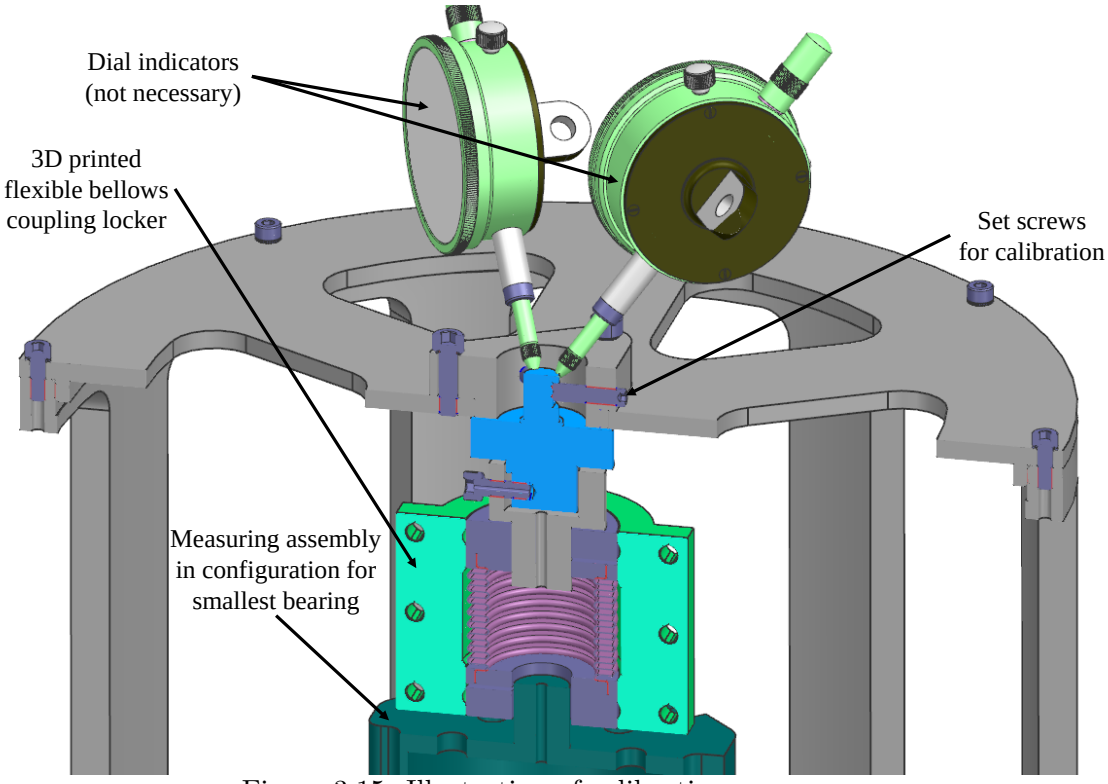

Figure 3.15: Illustration of calibration process.

If properly calibrated, the flexible bellows coupling is able to compensate which is axial and radial runout of the measured (tested) bearing as well as the bearing holding floating rotor (3.3.1). Coupling KB2/100-57-16-16 [22] was chosen for its material composition per requirement 3.1.0.2 (no plastic parts, that could outgas) and great radial stiffness.

Using FEM, torsion stiffness was calculated of the components in the chain of torque measurement. The results are in table 3.7. For more details about the analysis see the attached files.

Parameter	**Value**
Adapter [Nm/deg]	677
Compensator [Nm/deg]	7676
Flange [Nm/deg]	2227
Stand [Nm/deg]	1361
Flexible bellows coupling [Nm/deg]	119
Total [Nm/deg]	89

Table 3.7: Torsion stiffness of chosen components.

3.3.3 Thermal assembly

Thermal assembly (figure 3.16) sets the temperature of the tested bearing using external heating and cooling unit, for which a liquid feedthrough is used. The fluid loop is welded to the thermal baseplate. The pipe for fluid loop, as well as the thermal baseplate are made of copper to ensure good thermal conductivity. Fluid feedthrough, being already present at Honeywell, was not the component that would be chosen upon research, but rather design considerations were made around it, per requirement 3.1.0.1. The heating and cooling unit is being reused as well.

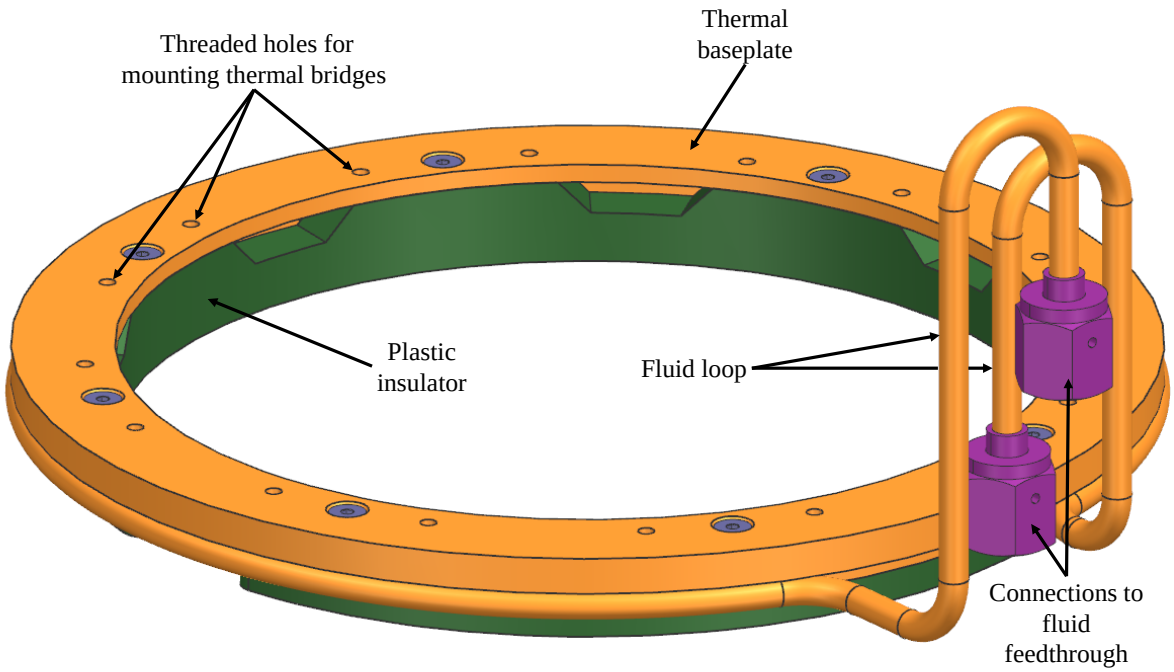

Figure 3.16: Thermal assembly.

The thermal baseplate then sits on a plastic insulator and has 16 mounting threaded holes for thermal bridges, that connects to the measured bearing stator and either transfers the heat into the bearing (for hot case) or takes heat from the bearing (for cold case).

Simple calculation was made, to determine if the entire thermal assembly, including thermal bridges, will be able to heat up or cool down the bearing, considering thermal resistance of each material. It was concluded, that for specified requirements 3.1.0.4 and 3.1.0.5, the assembly will be able to set the correct test conditions.

Around 3 watts (at temperature boundary conditions) are expected to transferred through the plastic insulator into the driving assembly's baseplate (3.3.1).

Thermal strap

Thermal straps (figure 3.17), made entirely from copper, have three parts - connector for the thermal plate, copper wire strand and connector for bearing. They are connected with screws on both sides, so they can be swapped quickly and easily to stay compatible with measuring assembly and they are used to transfer the heat (into or from) the bearing. Vacuum compatible thermal interface such as graphite pad should be used. They can be bought or custom made.

For current application, two custom variants are proposed, to better visualize the intended use. One variant can be seen used if figure 3.18.

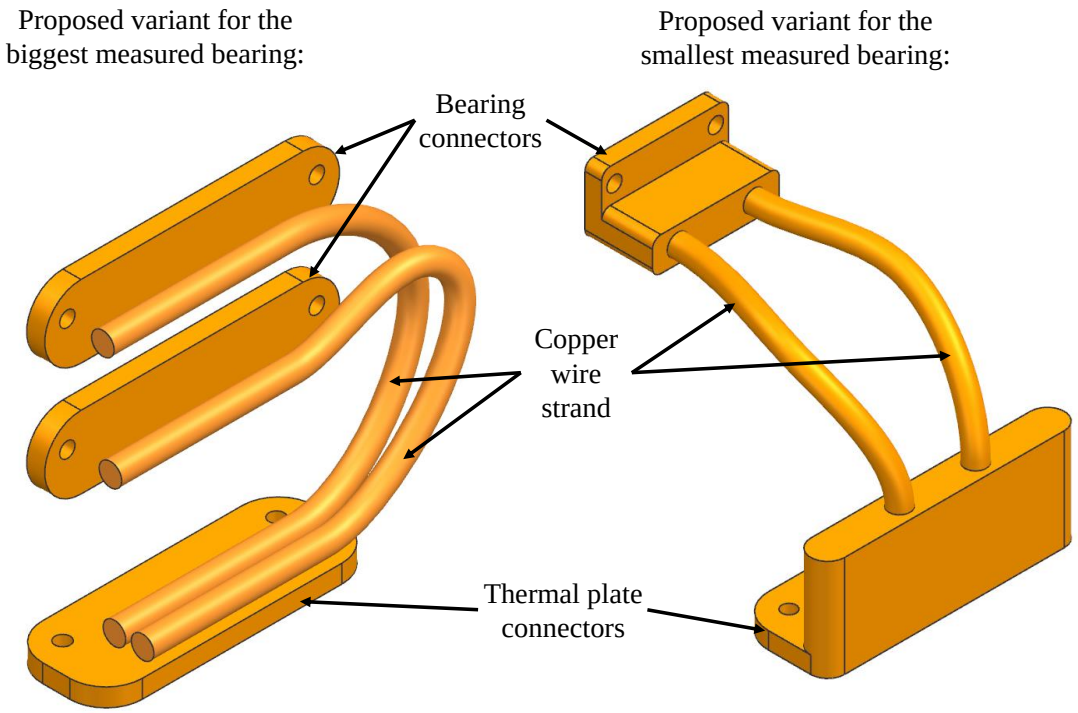

Figure 3.17: Thermal straps for proposed measuring assemblies.

Thermal straps are also designed in a way, that will not block the torque transfer to the torque sensor. This is ensured by slack built-in to the copper wire strand.

3.3.4 Measuring assembly

Measuring assembly is an assembly in which the tested bearing is secured. Its purpose is to connect to the driving assembly (3.3.1), torque sensor assembly (3.3.2) as well as thermal assembly (3.3.3) and can be seen in the top assembly in figure 3.18.

It can accept bearings in a wide range of diameters - the smallest inner diameter being 70 mm and the biggest outside diameter being 190 mm. Height was taken into consideration, although height limit was not set, since measuring assembly can be designed to fit bearings with height bigger than the current proposed variants. Theoretically, the maximum height is around 70 mm.

Theoretically it is possible to fit bearing with bigger outside diameter, but only if requirement 3.1.0.3 may not need to be met, since thermal straps cannot be used because of space constraining reasons.

For this thesis two variants of measuring assemblies are proposed to show, how the bearing can be mounted.

To mount the assembly, the rim is designed on part floating rotor in driving assembly (3.3.1) to make them concentric with measuring assembly. Assemblies are then secured together with M4 screws. There are multiple hole patterns for different mounting options and all of the holes are vented, so regular stainless steel screws can be used. Screws shall use locking washers to prevent loosening.

The entire measuring assembly must have maximal runout of 300 µm radially and 120 µm axially. The height of the Measuring assembly does not have to be precise, because the shaft of the measuring assembly, that is inserted into flexible bellows coupling, is used as a height compensator.

The smallest possible bearing assembly can be seen on figure 3.18 in the Top assembly with every component.

The meassuring assembly consists of a rotor and stator, with the bearings inner ring being the rotor and the outer ring being the stator. The torque generated by the rolling elements is being transferred through the stator into the torque sensor, that is stopping the rotation of the bearing. This rotor-stator distribution can be observed in figure 3.19, where the smallest possible bearing assembly is used. Thermal straps are included in the visualisation.

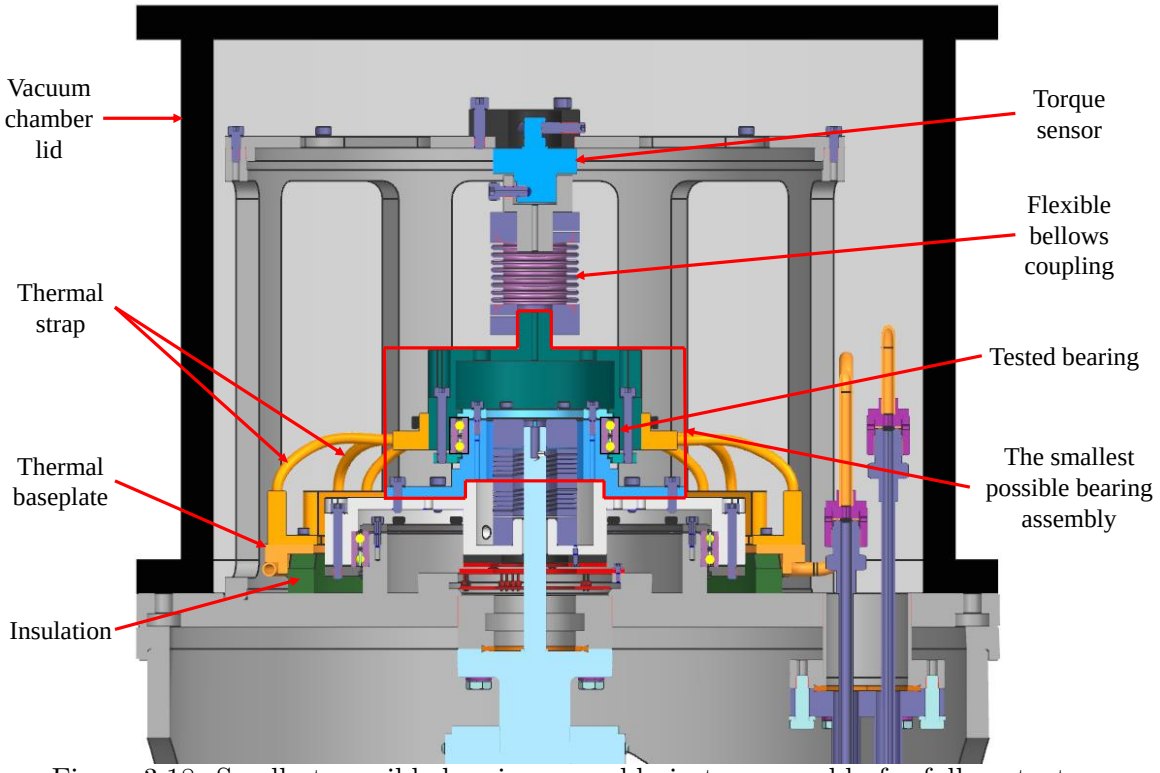

Figure 3.18: Smallest possible bearing assembly in top assembly for full context.

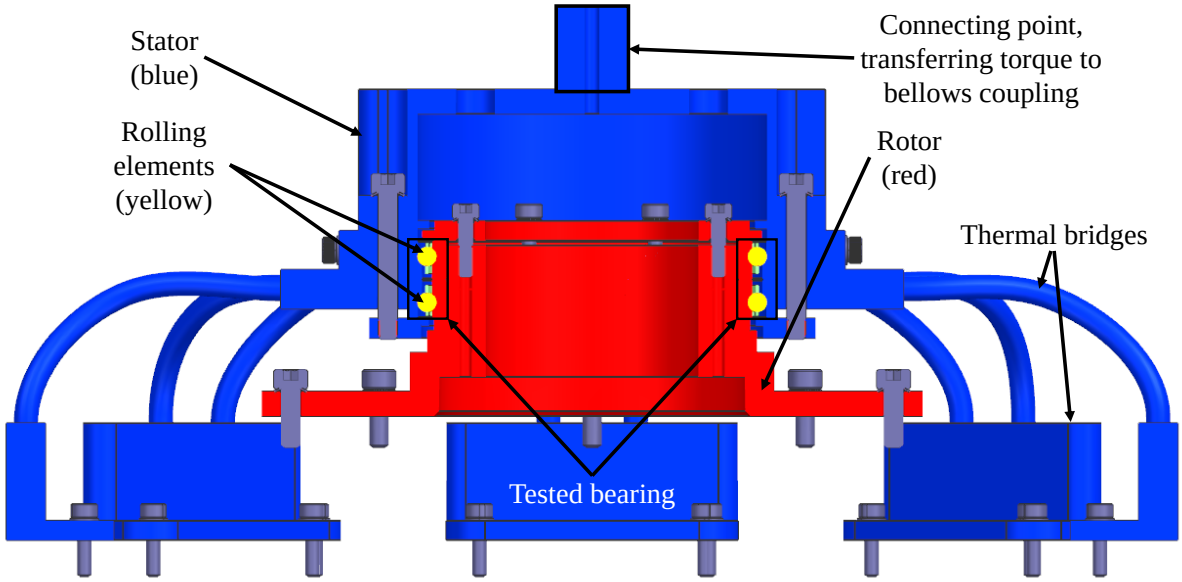

Figure 3.19: Visualisation of rotary (red) and stationary (blue) parts of the measuring assembly.

Smallest possible bearing assembly

This proposed assembly (figure 3.20) is comprised of four custom parts and the tested bearing - inner connecting ring, outer connecting ring and inner and outer securing rings. The outer connecting ring has mounting threaded holes for thermal straps and connects to the torque sensor assembly (3.3.2). Threaded holes for thermal straps are not vented, so special vented screws for vacuum must be used per requirement 3.1.0.9. The inner connecting ring is connected to the floating rotor in driving assembly (3.3.1).

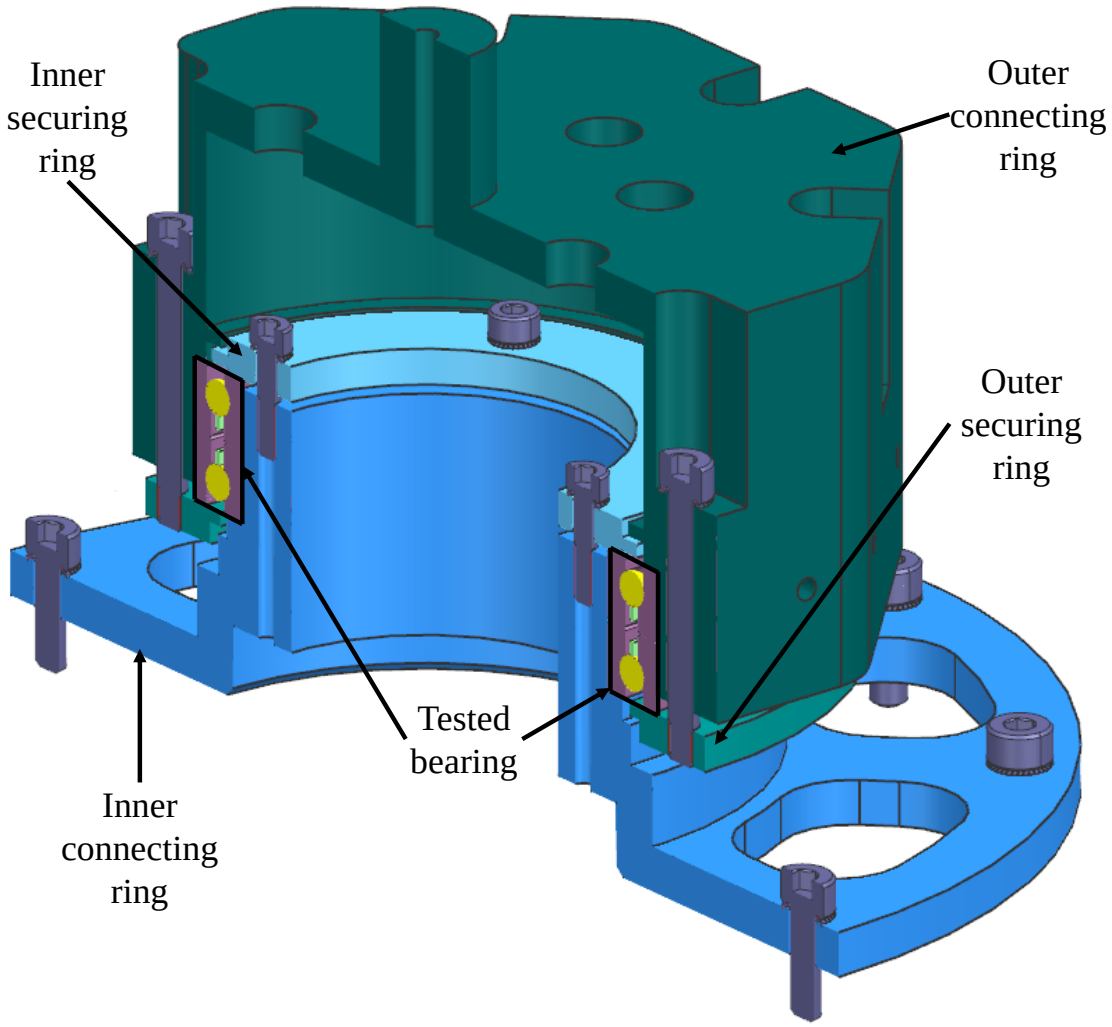

Figure 3.20: Smallest bearing proposed assembly.

For presentation SKF KDN.07008AR0 [23] bearing is used in back-to-back configuration.

Biggest possible bearing assembly

Just as the smallest possible bearing assembly, the biggest possible bearing assembly has four main parts and the tested bearing. All the necessary information is given in the page above. The color scheme of the biggest possible bearing assembly shown in figure 3.21 is the same as in figure 3.20, so refer to it for assembly description.

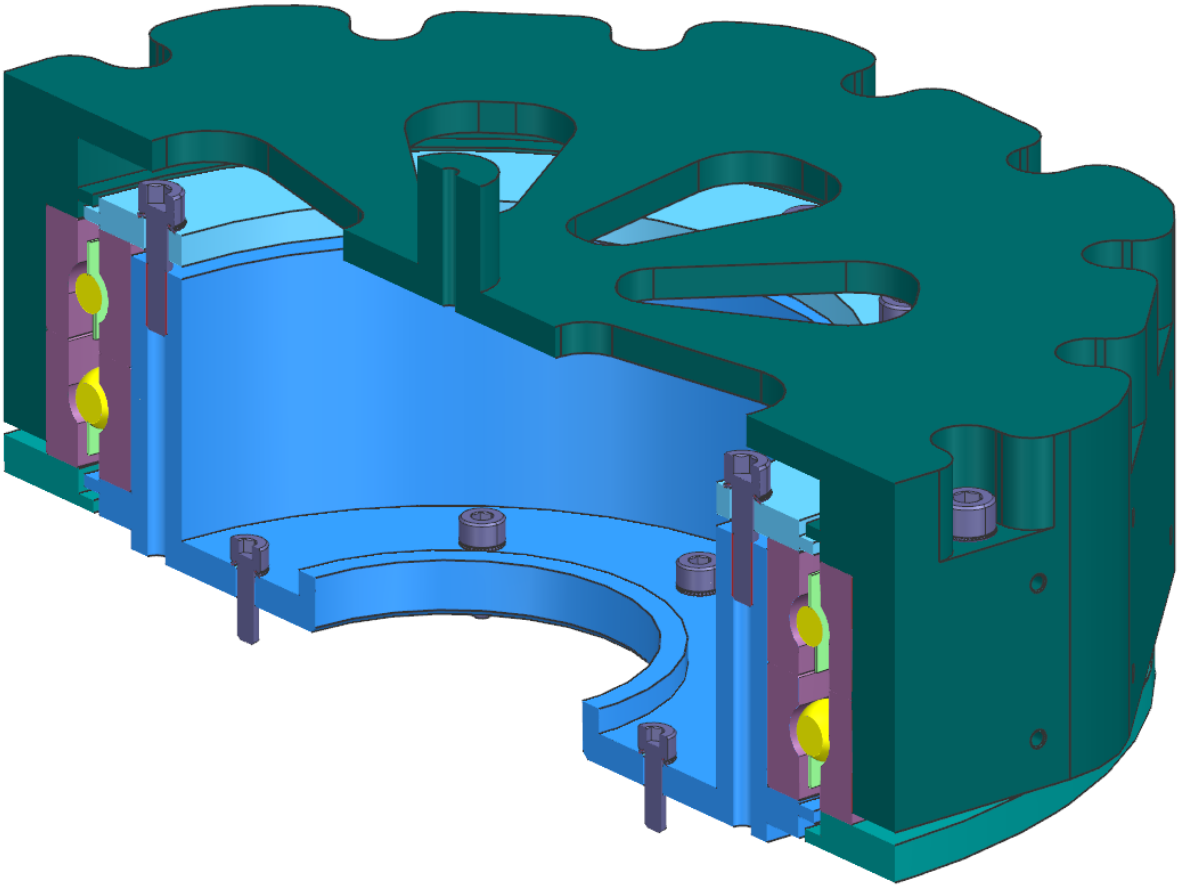

Figure 3.21: Biggest bearing proposed assembly.

For presentation SKF KDN.15020AR0 [24] bearing is used in face-to-face configuration.

4 Software

The software running on the Teensy 4.1 (section 3.2) is written in C++ using PlatformIO [25] extension and Arduino library [26] to make the workflow more efficient. For the torque sensor, Adafruit library [27] is used. A basic flowchart overview of the program algorithm is shown in figure 4.1.

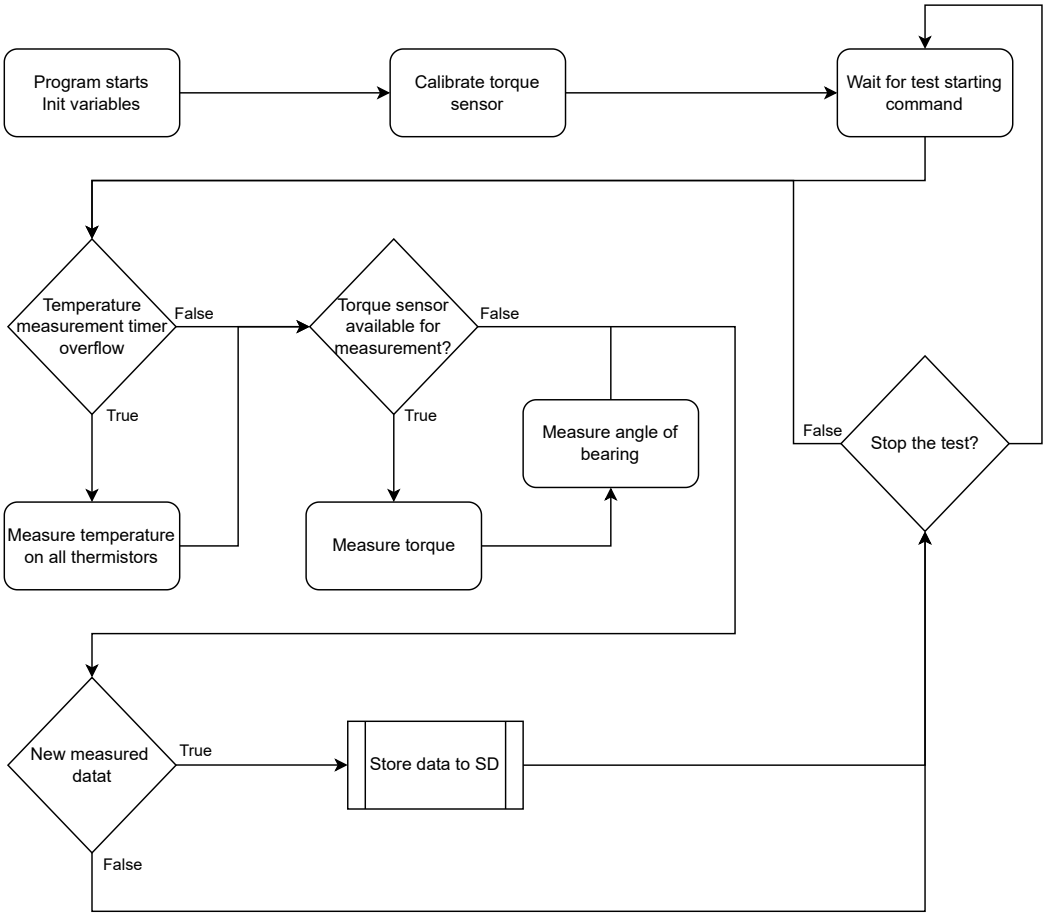

Figure 4.1: Program flowchart overview.

Measurement activation

The program starts, when the computer gets a command through a serial communication to start the measurement. The command to start the testing loop is *TEST*, and to end the testing loop, a *STOP* command needs to be sent. Serial communication is used for this purpose.

Measurement algorithm

The measurement is done at specified time intervals, that can be changed. For the temperature reading, the set sampling rate of 1Hz is used. The torque sampling rate is determined by the usage of the Adafruit library [27]. It has multiple options with the maximum sampling rate of 320 Hz. When torque is measured, the angle is measured as well, in order to pair these two sets of information together. SSI protocol is used to read the encoder data. The data is then stored on the SD card, but only if any value has changed. The precision of the measurement is listed at subsection 3.2.2.

Encoder data validity

If the data, that the encoder provides, is not valid, a value of -1000 is stored. The angle nominally has the values from 0° to 360°, so such a value is a strong indication of an error in measurement. The encoder determines the validity internally.

Data storage

Currently, the program stores all of the data to the Teensy's integrated SD card, but it can be programmed, with very little effort, to send the measured data directly to programs such as LabVIEW through serial communication, that is currently used to start and stop the test.

Because the Teensy 4.1 performs 64 bit double (and 32 bit float) operations in hardware, the double is used in calculation and data storage for better precision. With the maximal sampling rate of 320 Hz from the torque senor and encoder and 1 Hz from the thermistor, the test generates 5 128 bytes per second. If we add additional data such as data separators, 8 008 bytes per second are generated. That means, that the SD card with a capacity of 8 GB can store almost 280 testing hours.

5 Summary

In this thesis an analysis of bearing friction torque is performed in section 2.1, where a thought is given into how can the friction torque be affected. Then, in section 2.2, an analysis of possible ways to measure the torque is conducted, where a Wheatstone bridge is chosen as a method for the testing rig.

A test methodology is proposed in subsection 2.2.1 using two tests. First test measures the steady-state friction as a function of angular velocity and temperature, though the temperature dependency is not necessary and is only used to predict the behavior of the bearing with changing temperatures. The second test drives the bearing in an oscillatory manner and calculates the parameters of the Dahl's friction model using the function of steady-state friction determined in previous tests. The test can also be performed under different thermal conditions.

A testing rig was designed and it is thoroughly described in chapter 3, where in section 3.2 the electrical hardware is shown and in section 3.3 the mechanical hardware is explained. The software that runs on the DAB is briefly discussed in chapter 4.

The proposed solution reuses a lot of mechanical and electrical components per requirement 3.1.0.1, e.g. the vacuum chamber lid or the stepper motor controller. It can accept a variety of bearings, with the minimal inside diameter of 70 mm and maximal outside diameter of 190 mm. The motor is beneath the tested bearing and is not in a vacuum and therefore a rotary vacuum feedthrough is used. The measurement has an external heating and cooling unit connected via a fluid feedthrough. The testing rig measures the torque generated by the bearing, angle of the bearing and has eight channels for temperature measurement.

The current software could be improved by not only storing the data to the SD card, but also by sending them to other programs such as LabVIEW. Also, configurability could be improved, because currently, if a change in configuration (e.g. torque sensor sampling rate) is needed, a new program needs to be compiled with the necessary changes.

The current proposed measurement methodology could be extended to work with a more accurate model. For example, the current model works with 100% efficiency of hysteresis losses. In reality, that may not be true, so additional analysis and measurement can be designed to tackle this problem.

To summarize, as part of the thesis, all of the objectives were fulfilled and additional ideas how to further improve the thesis are given.

Bibliography

[1] CONLEY, Peter L. Design Valitadtion Part 2: Digital Simulation. In: *Space Vehicle Mechanisms*. John Wiley & Sons, Inc., 1998, pp. 705–720. ISBN 0-471-12141-X.

[2] SINGER, Herbert B. Ball Bearings. In: *Space Vehicle Mechanisms: Elements of Successful Design*. John Wiley & Sons, Inc., 1998, pp. 287–324. ISBN 0-471-12141-X.

[3] SINGER, Herbert B. Ball Bearings. In: *Space Vehicle Mechanisms*. John Wiley & Sons, Inc., 1998, p. 308. ISBN 0-471-12141-X.

[4] Components and materials. *SKF*. w.y. Available also from: `https://www.skf.com/us/products/rolling-bearings/principles-of-rolling-bearing-selection/general-bearing-knowledge/bearing-basics/components-and-materials`. [cit. 2024-05-18].

[5] Automotive torque measurement: A summary of seven different methods. *IEEE Vehicular Technology Conference*. 1982, vol. 32nd, no. 1, pp. 71–76. Available from DOI: `10.1109/VTC.1982.1623003`.

[6] The genesis of the Wheatstone bridge. *Engineering Science and Education Journal*. 2001, vol. 10, no. 1, pp. 37–40. Available from DOI: `10.1049/esej:20010106`.

[7] Wheatstone bridge. *Wikipedia: the free encyclopedia*. w.y. Available also from: `https://en.wikipedia.org/wiki/Wheatstone_bridge%5C#/media/File:Wheatstonebridge.svg`. [cit. 2024-05-18].

[8] SKALICKÝ, Jiří. *Elektrické regulované pohony*. Brno, 2007. Available also from: `https://moodle.vut.cz/pluginfile.php/836642/mod_resource/content/1/El._reg._pohony.pdf`. [2024-05-17]. Available to mechatronics bachelor students at the Brno University of Technology, Faculty of Mechanical Engineering.

[9] OLSSON, H. et al. Friction Models and Friction Compensation. *European Journal of Control*. 1998, vol. 4, no. 3, pp. 176–195. Available from DOI: S0947-3580(98)70113-X. [cit. 2024-05-23].

[10] *Epsilon2 - Rotary Actuator For Space Applications: Testing Device For Rolling Elements Bearing of Rotary Actuator*. 2018. Available also from: https://www.vut.cz/vav/projekty/detail/27493. [2024-05-17]. Honeywell confidential document, for internal use only.

[11] Teensy 4.1. *PJRC*. [2020]. Available also from: https://www.pjrc.com/store/teensy41.html. [cit. 2024-05-18].

[12] *KiCad EDA*. 2024. Available also from: https://www.kicad.org/. [cit. 2024-05-23].

[13] Metric, Non-Rotating, Shaft Mount, Reaction Torque Sensors. *Omega*. ©1996 - 2024. Available also from: https://www.omega.com/en-us/force-and-strain-measurement/torque-sensors/tqm201/p/TQM201-1#. [cit. 2024-05-17].

[14] NAU7802 24-Bit ADC. *Adafruit*. w.y. Available also from: https://www.adafruit.com/product/4538. [cit. 2024-05-18].

[15] IncOder CORE – Lightweight Encoder. *Celera Motion*. w.y. Available also from: https://www.celeramotion.com/zettlex/product/incoder-core/. [cit. 2024-05-18].

[16] Převodník TTL na RS422, MAX490 Full Duplex. *LaskaKit*. ©2024. Available also from: https://www.laskakit.cz/prevodnik-ttl-na-rs422--max490-full-duplex/%5C#relatedFiles. [2024-05-23].

[17] Převodník logických úrovní I2C 5V na 3V. *LaskaKit*. ©2024. Available also from: https://www.laskakit.cz/prevodnik-logickych-urovni-i2c-5v-na-3v/. [cit. 2024-05-23].

[18] RTS Series Ring Terminal Temperature Sensor. *Mouser*. 2023. Available also from: https://cz.mouser.com/datasheet/2/18/1/AAS_EXA_920_801E_RTS_Series_101123_web_1-3358796.pdf. [cit. 2024-05-18].

[19] Magnetically coupled rotary feedthrough, motorized, DN 40 CF. *Pfeiffer-vacuum*. ©2024. Available also from: https://www.pfeiffer-vacuum.com/global/en/shop/products/420MRM040_M. [cit. 2024-05-19].

[20] 8SMC5-USB - Stepper DC Motor Controller. *Standa*. ©2000 - 2024. Available also from: https://www.standa.lt/products/catalog/motorised_positioners?item=525. [cit. 2024-05-21].

[21] KDN.K15008AR0. *SKF*. w.y. Available also from: https://www.skf.com/cz/productinfo/productid-KDN.K15008AR0. [cit. 2024-05-19].

[22] Miniature Metal Bellows Coupling. *Kbk-antriebstechnik*. 2021. Available also from: https://www.kbk-antriebstechnik.de/fileadmin/user_upload/02_produkte/01_metallbalgkupplungen/03_datenblaetter_englisch_metallbalgkupplungen/metallbalgkatalog_datenblatt_kb2_englisch.pdf. [cit. 2024-05-19].

[23] KDN.K0708AR0. *SKF*. w.y. Available also from: https://www.skf.com/mk/productinfo/productid-KDN.K07008AR0. [cit. 2024-05-18].

[24] KDN.K15020AR0. *SKF*. w.y. Available also from: https://www.skf.com/au/products/thin-section-bearings/reali-slim-thin-section-bearings/productid-KDN.K15020AR0. [cit. 2024-05-19].

[25] *PlatformIO*. w.y. Available also from: https://platformio.org/. [cit. 2024-05-23].

[26] ArduinoCore-avr. *Arduino*. [2022]. Available also from: https://github.com/arduino/ArduinoCore-avr/tree/master/cores/arduino. [cit. 2024-05-23].

[27] Adafruit_NAU7802. *Adafruit*. 2023. Available also from: https://github.com/adafruit/Adafruit_NAU7802. [cit. 2024-05-23].

List of abbreviations

ADC Analog to Digital Converter. 13, 14, 21, 22, 24

BUT Brno University of Technology. 16, 21

CAD Computer-Aided Design. 16, 26, 30, 46

DAB Data Acquisition Board. 19, 20, 23, 25, 26, 41, 47

EHD Elastohydrodynamic lubrication. 10, 11

ENOB Effective Number of Bits. 21, 22

FEM Finite Element Method. 8, 9, 32

FS Full Scale. 22

FSO Full-Scale Output. 22

NTC Negative Temperature Coefficient. 24, 25, 46

PCB Printed Circuit Board. 18–20, 24, 46

RPM Revolutions Per Minute. 11, 16, 18, 23

List of Figures

List of attachments

The attached files include the mechanical drawings of all designed parts, step file of the testing rig excluding Honeywell parts, drawing of DAB as well as it's step file and the software that runs on it. Additionally, the files include the results of the supporting bearing (3.3.1) analysis.

The file structure in *2024_Attached_files_Lachman_Ivo_238718* is as follows:

Folder	**File or subfolder**	**Description**
\10Electrical		
	\DAB.step	*Step file (AP214) of the DAB with components.*
	\DAB_schematic.pdf	*Electrical drawing of the DAB.*
\20Mechanical		
	\10Drawings	*Folder with mechanical drawings of all the designed components.*
	\20Bearing_analysis	*Folder with bearing analysis documents.*
	\ASSEMBLY,TOP LEVEL.stp	*Step file (AP214) of the top assembly level without the Honeywell components.*
	\Structural_analysis.pdf	*Analysis of the system torsion stiffness.*
\30Software		*Folder including all of the files PlatformIO has generated as well as the software for DAB (including all of the libraries.)*